**International Journal of Power Electronics and Drive System (IJPEDS)**
Vol. 8, No. 1, March 2017, pp. 156~166
ISSN: 2088-8694, DOI: 10.11591/ijpeds.v8i1.pp156-166


# A Novel Sensorless Initial Rotor Position Estimation Method for Permanent Magnet Synchronous Motors

**Chien Feng Wu[1], Shir Kuan Lin[2]**
[1-2] Department of Electrical Engineering, National Chiao Tung University, Taiwan, Province of China

**Article Info**

***Article history:***

Received Oct 03, 2016
Revised Dec 09, 2016
Accepted Dec 19, 2016

***Keyword:***

High frequency signal injection
Initial rotor position estimation
Optimal injection frequency
PMSM

**ABSTRACT**

This paper presents a high efficiency initial rotor position estimation method for Permanent Magnet Synchronous Motors (PMSM). The approach uses the viable inductance model to analyze the optimal motor injection sine wave frequency as the motor's test signal. Unlike other high-frequency injection methods, this approach does not require trial and error experiments. The injection frequency is identified by programmable simulations using Matlab. Experimental evaluation of 3-phase PMSM showed that this injection frequency optimization method works successfully. The proposed method can find the optimal injection frequency without experimentation, and outperforms other test signals in terms of accuracy, vibration quantity and noise. This microprocessor-developed 3-phase PMSM control driver can be applied to electrical appliances, machine tools and automation.



***Corresponding Author:***

Shir-Kuan Lin,
Department of Electrical Engineering,
National Chiao Tung University,
Taiwan, Province of China.
Email: sklin@mail.nctu.edu.tw

## 1. INTRODUCTION

Sensorless Permanent-Magnet (PM) motors are commonly used in industrial machinery and home appliances. Their advantages include a simple structure, good reliability, high power density, good efficiency and low maintenance costs. In addition, such motors will not be damaged by arcing or friction at high-speed rotation. PM motors use non-contact phase commutation instead of mechanical phase-changing devices such as brushes. To activate and rotate the PM motor smoothly, position sensors are needed to detect the rotor position. Position sensors can be photo- or magnet-based, but rotor position detection may be costly and unreliable.

Implementing motor control without position sensors can enhance the reliability and reduce the cost of motor sensors. In a motor control system, rotor position must be known to obtain better control performance. In recent years, several methods have been developed to estimate rotor position, including the counter electromotive method [1]-[4], the extended Kalman filter [5],[6], the artificial neural networks [7], Finite Element method [8],[9] and sliding mode current observer [10]-[12]. These methods are based on modern control theory and realized through the use of microprocessors.

However, these methods can only work when the rotor is rotating. As noted by Haque [13], when the rotor is still, measuring the initial position of the rotor is difficult in several respects: 1) A still motor produces no electrical-field or magnetic-field change which can be measured to evaluate rotor-position, 2) position estimation is load dependent [14], and 3) it entails high calculation complexity and sophisticated hardware requirements [15].

In 1996, Matsui [16] reviewed five methods of estimating the initial position of sensorless PM brushless DC motor, including: 1) Auxiliary sensors, 2) open loop controls, 3) specific gate patterns, 4) arbitrary starting and 5) salient-pole motors. Compared with Methods 2) - 4), Method 5) starts the motor

more smoothly and prevents reverse rotation. Method 5) is mainly based on the magnetic saturation of the magnetic conductive material. The test signal, voltage or current are applied to the motor, and then the difference of the corresponding current peak value is measured to calculate the current position and rotation speed of the rotor [17]. In practice, to maintain the rotor position at standstill, the energy within the motor must be offset. Once the test signals are input, an identical counter-directional signal must be input to zero out the net torque. This signal injection method is referred to as the Salient Pole method.

The Salient Pole method can avoid undesirable events such as rotor back-kicking or rotor oscillation prior to smooth running, making this method superior to the other four methods. Based on the Salient Pole method, several approaches are provided to further enhance the precision of initial-position estimation. In research on the Salient Pole method, Schmidt et al. [18] established a table of input-voltages and corresponding peak currents of a motor. When the motor starts, a three-phase voltage is applied to it. The induced peak current is then measured and the initial position of the rotor can be obtained based on the table. Tursini et al. [19] found that evaluations of rotor position based only on peak current are subject to several uncertainties. They proposed an improved method which applies the same voltage waveform 16 to measure the feedback current, using fuzzy theory to determine rotor position, resulting in estimations with errors of less than 20 degrees.

Hatakeyama [20] evaluated the rotor position by applying two sine waves. The amplitude of the first high-frequency sine wave is small, so the rotor remains still. However, the amplitude of the second sine wave is high, providing sufficiently strong magnetic saturation. Since the first sine wave cannot induce a strong current, the detected rotor position cannot be determined to be in the one-to-two quadrant or the three-to-four quadrant. Hence the second sine wave is applied to determine the quadrant of the rotor position. However, the strong second sine wave will result in some rotor rotation.

## 2. RESEARCH METHOD

The line inductance of a PMSM, denoted by $L_t$, can be described as $L_t = L_{eq} + L_{end}$ where $L_{eq}$ is the 2-D equivalent inductance and $L_{end}$ is the end-turn inductance of windings. $L_{end}$ is caused by three-dimensional (3-D) magnetic flux in a PMSM, and is usually much less than $L_{end}$. Thus, this paper is concerned only with $L_{eq}$. Some assumptions are listed here to simplify the analysis.

The line inductance of a PMSM, denoted by $L_t$, can be described as $L_t = L_{eq} + L_{end}$ where $L_{eq}$ is the 2-D equivalent inductance and $L_{end}$ is the end-turn inductance of windings. $L_{end}$ is caused by three-dimensional (3-D) magnetic flux in a PMSM, and is usually much less than $L_{end}$. Thus, this paper is concerned only with $L_{eq}$. Some assumptions are listed here to simplify the analysis.

A1. We ignore the eddy current effect on inductance.
A2. The shape of the shoes, the teeth and the slots of the stator is simplified as rectangular shapes.
A3. For the calculation of the air-gap permeance, the field pattern assumes that the flux lines are always orthogonal to the intersection surface of the air-gap and the steel.
A4. The B-H curve of the PM is linear with the constants of the relative permeability ( $\mu_r$ ) and the remanence ( $B_r$ ).
A5. The relative permeability of the rotor and the stator back iron are infinite ( $\mu_{Fe} = \infty$ ), and the nonlinear interaction of these two fields is considered only to calculate the air-gap inductance.
A6. The input coil current is constant.

As shown in Figure 1, in this paper, all three phases are excited by different winding currents, as opposed to the approach used in [21]. It is known that $L_{eq}$ is the sum of the air-gap ( $L_g$ ) and the slot inductances ( $L_{slot}$ ).

$$L_{eq} = (L_g + L_{slot})\frac{N_s}{3} \quad (1)$$

B where $N_s$ is the total number of slots, and the denominator 3 is the number of the phases of a PMSM. The inductances $L_g$ and $L_{slot}$ are respectively functions of the flux linkage $\Phi_g$ and $\Phi_s$.

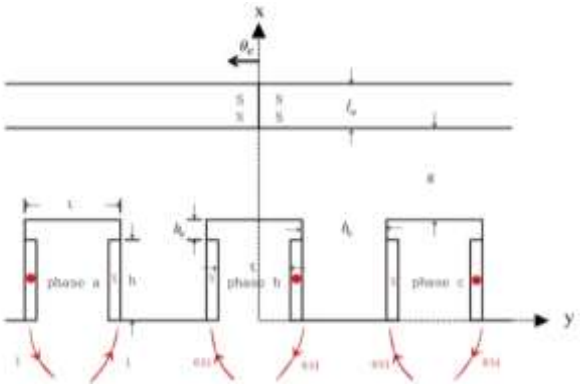


Figure 1. Simplified shoes, teeth, and slots structure

Figure 2 shows the flux linkages of the windings divided into five parts: $\Phi_g$, $\Phi_{s1}$, $\Phi_{s2}$, $\Phi_{s3}$ and $\Phi_{s4}$, where $\Phi_g$ is the flux crossing the air-gap, while $\Phi_s$ consists of $\Phi_{s1}$, $\Phi_{s2}$, $\Phi_{s3}$ and $\Phi_{s4}$.

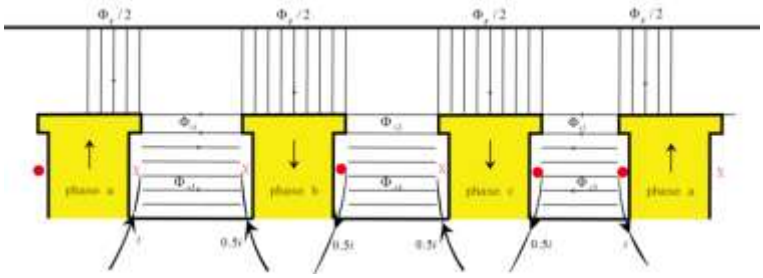


Figure 2. Flux pattern of winding current

The $L_{slot}$ can also be divided into four parts as:

$$L_{slot} = 2L_{s1} + L_{s2} + 2L_{s3} + L_{s4} \quad (2)$$

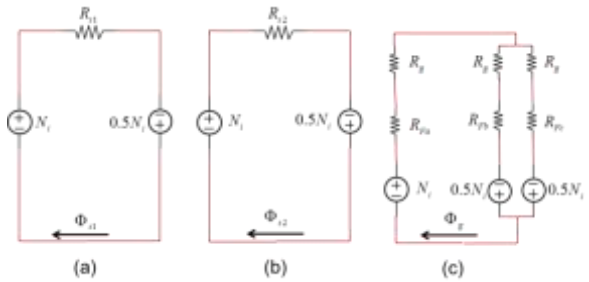


Figure 3. (a) equivalent magnetic circuit of $\Phi_{s1}$. (b) equivalent magnetic circuit of $\Phi_{s2}$. (c) Equivalent magnetic circuit of air-gap flux

Figure 3(a) and (b) respectively show the equivalent magnet circuits of $\Phi_{s1}$ and $\Phi_{s2}$. Note that $N$ is the number of turns of each stator tooth, $R_{s1}$ is the magnetic reluctance of $\Phi_{s1}$, and $R_{s2}$ is the magnetic

reluctance of $\Phi_{s2}$. It follows from Figure 3 that $\Phi_{s1}=3Ni/2R_{s1}$. According to the definition of the inductance, we obtain

$$L_{s1}=\frac{3}{2}N\frac{d\Phi_{s1}}{di}=\frac{9}{4}\frac{N^2}{R_{s1}} \tag{3}$$

It is well known that $R_{s1}=b_0/\mu_0 h_0 z$, where $b_0$ and $h_0$ are defined in Figure 1 The current direction of faces b and c are the same, therefore $\Phi_{s2}$ and $L_{s2}$ are almost equal to zero:

$$\Phi_{s2}\approx 0 \quad L_{s2}\approx 0 \tag{4}$$

In Figure 2, i.e., the slot between the teeth of phases b and c. The magnetic motive force (MMF) at the top of the slot is equal to $2N_i$, while it is zero at the bottom. This is because the turns are uniformly distributed in the slot, and the magnetic field $H_{s3}(x)$ crossing the slot increases linearly from the bottom of the slot to the top. Since $H_{s3}(0)=0$ and $H_{s3}(h)=2Ni/(b_0+\tau-t)$, we have $H_{s3}(x)=3Ni/2[(b_0+\tau-t)h]$, where $x$ is the distance from the bottom of the slot (see Figure 2).

This allows us to express $L_{s3}$ from the energy viewpoint as

$$L_{s3}=\frac{\int_{VOL}\mu_0 H_{s3}^2 dV}{i^2}=\frac{3}{4}\frac{\mu_0 N^2 hz}{(b_0+\tau-t)} \tag{5}$$

It is well known that $L_{s4}\approx L_{s2}$, therefore $\Phi_{s4}$ and $L_{s4}$ are almost equal to zero:

$$\Phi_{s4}\approx 0 \quad L_{s4}\approx 0 \tag{6}$$

The equivalent magnetic circuit in Figure 3(c) describes the air-gap flux $\Phi_g$ that goes from the shoe of phase a to the reluctance of phase a $R_{Fa}$ and the PM reluctance $R_g$, then 1/2 $\Phi_g$ separately pass through reluctance of phase a and phase b. $R_{Fa}$, $R_{Fb}$, $R_{Fc}$ and $R_g$ can be approximated as:

$$\begin{aligned}
R_g &= \frac{l_m}{\mu_r\mu_0\tau z}+\frac{g}{\mu_0\tau z}\\
R_{Fa} &= \frac{h_0}{\mu_r\mu_{a1}(B_{a1})\tau z}+\frac{h}{\mu_0\mu_{a2}(B_{a2})tz}\\
R_{Fb} &= \frac{h_0}{\mu_r\mu_{b1}(B_{b1})\tau z}+\frac{h}{\mu_0\mu_{b2}(B_{b2})tz}\\
R_{Fc} &= \frac{h_0}{\mu_r\mu_{c1}(B_{c1})\tau z}+\frac{h}{\mu_0\mu_{c2}(B_{c2})tz}
\end{aligned} \tag{7}$$

$\mu_{a1}$, $\mu_{b1}$, $\mu_{c1}$ are the relative degrees of permeability in the tooth, and $\mu_{a2}$, $\mu_{b2}$, $\mu_{c2}$ are those in the shoe. It then follows from Figure 3(c) that $\Phi_g=3Ni/2[R_g+R_{Fa}+R_{ss}]$ $R_{ss}=(R_g+R_{Fb})(R_g+R_{Fc})/(R_g+R_{Fb})+(R_g+R_{Fc})$. Thus

$$L_g=\frac{3}{2}N\frac{d\Phi_g}{di}=\frac{9}{4}\frac{N^2}{[R_g+R_{Fa}+R_{ss}]} \tag{8}$$

However, by assumption A5, the relative permeability of the stator back iron is a nonlinear function of the flux densities in the shoes and the teeth of the stator. These flux densities are defined as follows:

$$B_{a1}=\frac{\Phi_{ma}+\Phi_g+\Phi_{sa}}{\tau z} \quad B_{a2}=\frac{\Phi_{ma}+\Phi_g+\Phi_{sa}}{tz}$$
$$B_{b1}=\frac{\Phi_{mb}-\Phi_g/2+\Phi_{sb}}{\tau z} \quad B_{b2}=\frac{\Phi_{mb}-\Phi_g/2+\Phi_{sb}}{tz}$$
$$B_{c1}=\frac{\Phi_{mc}-\Phi_g/2+\Phi_{sc}}{\tau z} \quad B_{c2}=\frac{\Phi_{mc}-\Phi_g/2+\Phi_{sc}}{tz} \tag{9}$$

where $\Phi_m$ are the fluxes of the PM flowing through the three phase. $\Phi_s$ are the equivalent slot linkage fluxes of the three phases.

It is easy to calculate $\Phi_{ma}$, $\Phi_{mb}$, $\Phi_{mc}$, $\Phi_{sa}$ $\Phi_{sb}$ $\Phi_{sc}$ with the following equations:

$$\Phi_{ma}=z\int_l B_{mga}dl \quad \Phi_{mb}=z\int_l B_{mgb}dl \quad \Phi_{mc}=z\int_l B_{mgc}dl$$
$$\Phi_{sa}=\frac{L_s i}{2N} \quad \Phi_{sb}=-\frac{L_s i}{4N} \quad \Phi_{sc}=-\frac{L_s i}{4N} \tag{10}$$

It is apparent that flux densities are functions of $\Phi_g$, so the flux $\Phi_g$ should make the following error function $E(\Phi_g)$ zero from the equivalent circuit shown in Figure 3 (c):

$$E(\Phi_g)=\frac{3}{2}Ni-\Phi_g[R_g+R_{Fa}+R_s]\approx 0 \tag{11}$$

$E(\Phi_g)$ is a nonlinear equation with a single variable $\Phi_g$. Applying the iteration method to the above equation, we can easily obtain $\Phi_g$ that makes $E(\Phi_g)\approx 0$, provided that $\Phi_m$ is known.

We substitute the flux $\Phi_g$ into (8) to calculate the air-gap equivalent inductance $L_g$. The slot inductance $L_{slot}$ and the air gap inductance $L_g$ can be substituted into Eq. 1 to calculate the magnetic saturation and the motor's effective equivalent inductance $L_{eq}$. Finally, substitute into (1) to obtain $L_{eq}$

Figure 1 shows the d-q winding model of a PMSM. In this figure, 1d and 1q represent the armature d-q windings, 2d the constant field winding corresponding to the permanent magnet mounted on the rotor and 3d and 3q the equivalent windings for eddy current. In this paper, the iron loss arises from the resistance of the equivalent winding for eddy current [1].

## 3. ROTOR POSITION ESTIMATION METHOD

As noted in [2], the motor inductance changes with the rotor angle, thus the relationship between the inductance value and the current can be written as:

$$v=L\frac{di}{dt} \tag{12}$$

When the voltage is kept constant in the above formula, the inductance value is inversely proportional to the current differential, so the rotor position can be determined by calculating the difference of the inductance value from the speed of the current response.

As shown in Figure 4, the drive circuit of the three-phase permanent magnet synchronous motor is a three half-bridge circuit. We use a three-phase leg with a total of six transistors and flywheel diodes ( $S_1$ and $S_2$, $S_3$ and $S_4$, $S_5$ and $S_6$) to form a three-phase inverter, where $v_a$ is the input voltage of phase a, $v_b$ is the input voltage of phase b, $v_c$ is the input voltage of phase c, the neutral point voltage at the intersection of the three phases is $v_n$ and $V_{dc}$ is the DC voltage source. The three-phase permanent magnet synchronous motor coil $Y$ passes phase a as phase current $i_a$, phase b as phase current $i_b$, and phase c as phase current $i_c$.

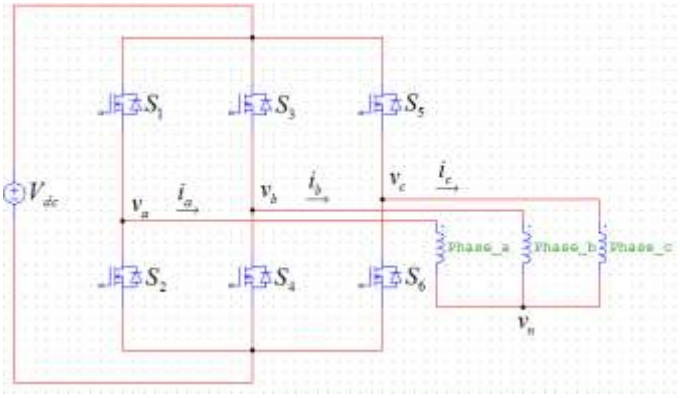


Figure 4. Three-phase motor and drive circuit

The three-phase voltage input method includes six modes, where the a-phase injection definite voltage signal mode is taken as an example:

$$v_{ab}(\equiv v_{an}-v_{bn})=v_{ac}(\equiv v_{an}-v_{cn})=V_{dc}$$
$$i_a=i_{a(+)}\text{、}\quad i_b=i_c=-(1/2)i_{a(+)} \tag{13}$$

where $V_{dc}$ is the signal amplitude

$$v_{ab}=V_{dc}=\frac{3}{2}R_s i_{a(+)}+\frac{3}{2}(L+M)\frac{d}{dt}i_{a(+)} \tag{14}$$

Similarly, assuming the a-phase injection is a negative voltage signal mode

$$v_{ab}=-V_{dc}=\frac{3}{2}R_s i_{a(-)}+\frac{3}{2}(L+M)\frac{d}{dt}i_{a(-)} \tag{15}$$

The positive value's square wave test signal $V_{dc}$ is input to the motor model, the simplified resistance is $\frac{3}{2}R_s=R$ and the signal is the positive inductance value.

Thus we can rewrite (13) as a voltage signal relationship

$$v_{ab}=V_{dc}=i_{a(+)}R+L_{eqa(+)}\frac{di_{a(+)}}{dt} \tag{16}$$

$$i_{a(+)}(t)=\frac{V_{dc}}{R}(1-e^{-t/\tau a(+)})\text{ , }\tau_{a(+)}=L_{eqa(+)}/R \tag{17}$$

The negative value's square wave test signal $-V_{dc}$ is input into the motor model. The negative signal input uses the negative inductance value $L_{eq(-)}$; similarly, the voltage is

$$v_{ab}=-V_{dc}=i_{a(-)}R+L_{eqa(-)}\frac{di_{a(-)}}{dt} \tag{18}$$

The current response equation is:

$$i_{a(-)}(t)=\frac{-V_{dc}}{R}(1-e^{-t/\tau a(-)})\text{ , }\tau_{a(-)}=L_{eqa(-)}/R \tag{19}$$

We set a current sampling time $t_p$, the negative current $i_{(-)}(t_p)$ and positive current $i_{(+)}(t_p)$. Subtracting the absolute values from each, the three-phase current difference $\Delta i$ is:

$$\begin{cases} \Delta i_a = |i_{a(-)}(t_p)| - |i_{a(+)}(t_p)| \\ \Delta i_b = |i_{b(-)}(t_p)| - |i_{b(+)}(t_p)| \\ \Delta i_c = |i_{c(-)}(t_p)| - |i_{c(+)}(t_p)| \end{cases} \quad (20)$$

Through this method, we can use the magnitude relationship of the three $\Delta i$ values to separate the 360 degree electrical angle into six parts, each with an electrical angle resolution of sixty degrees, as shown in Figure 5 In an electrical angle of 30 degrees $\Delta i_b$ and $\Delta i_c$ rise and fall nearly linearly, making this area a dividing point, and the other five blocks are treated with the same logic.

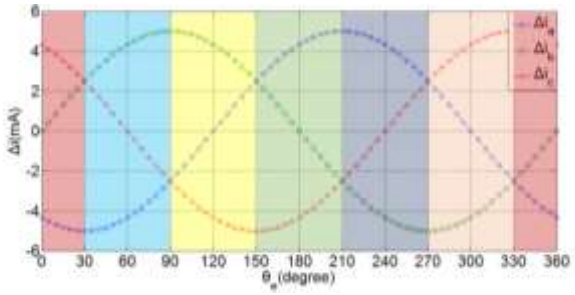


Figure 5. Electrical angle partioning

This square-wave method can be used to successfully identify the initial rotor position. However, if the motor has a large stator coil resistance value, the current response will be little changed, resulting in an excessively large judgment error in determining the initial rotor position. Therefore, this paper seeks to select an appropriate injection frequency to maximize the current distance and minimize the rotor position estimation error.

## 4. OPTIMUM FREQUENCY SEARCH

The proposed optimum frequency search method is described in following flow chart. Figure 6 illustrates the process of determining the optimal injection frequency. The first step is to input the motor's geometric parameters. Step 2 sets the coil's initial current value. Of particular note, the coil current $i_{(n)}$ is not arbitrary, but is rather determined iteratively. The current iteration calculation seeks to determine the optimal current $i_a(f_{optimal})$ as we approach the optimal frequency $f_{optimal}$, and thus calculate the circuit current $i_{(n)}$ at the time of analysis to optimize the accuracy of current value calculations.

Step 3 inputs the data produced in Steps 1 and 2 to the model derived in Section 2 to calculate the motor's equivalent inductance.

Step 4: The optimal injection frequency search method inputs different frequency sine wave signals (from 1Hz to 500Hz). When the voltage $v_s$ is positive, $L_{eqa(+)}(\theta_e)$ is the inductance value; when $v_s$ is negative, $L_{eqa(-)}(\theta_e)$ is the inductance value, and this signal is input into the Simulink motor model. Subtracting the absolute value of the half-cycle coil current $i_{(+)}$ from the negative half cycle coil current $i_{(-)}$ obtains $\Delta i$, and the frequency at which the maximum current $\max(\Delta i_a)$ occurs is the optimal current $f_{optimal}$

Finally, compare the optimal frequency current and the current at the time. If they are not similar, then add a current error $i_{error}$ and continue with further iterations. If they are similar, terminate the operation with the optimal frequency simulation. Where the current error value $i_{error}$ is $(i_{opt} - i_{(n)})/2$, if they are almost equal, the operation terminates to complete the optimal frequency search.

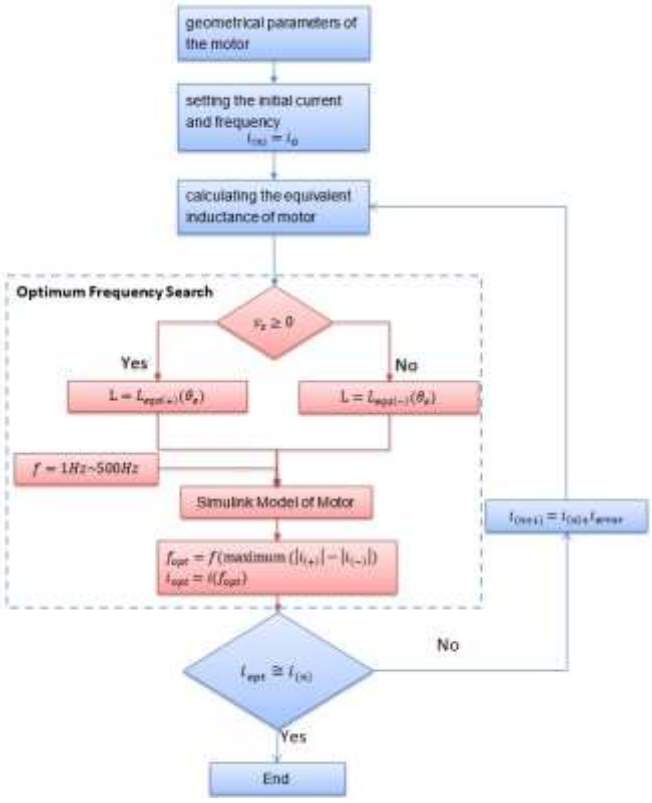


Figure 6. Flow chart of optimum frequency search

Figure 7 shows the result of the frequency search from 1Hz to 500Hz. The largest $\Delta i$ occurs at 21Hz, followed by 20.05mA.

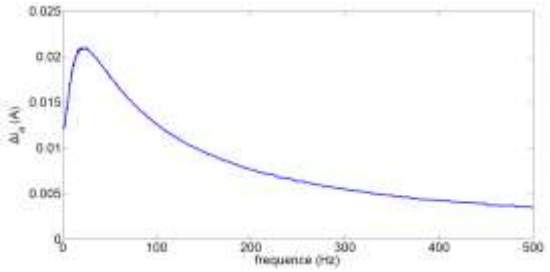


Figure 7. Result of frequency search

## 5. EXPERIMENTAL RESULTS

Experiments used three-phase, 16-pole, and 9-slot PMSMs, with microcontrollers to produce the injection signal and measure the coil current to verify the simulation results. The injection signal is a sinusoidal function with a peak value of 75 V. To find the optimal input sign wave, the frequency of the input signal was increased from 10 Hz to 50 Hz. The relation between the three-phase current difference ( $\Delta i$ ) and the rotation angle is shown in Figure 8 The amplitude of the three-phase current difference ( $\Delta i$ ) is maximized when the frequency of input sin wave is 20 Hz. This result is identical to the simulation result.

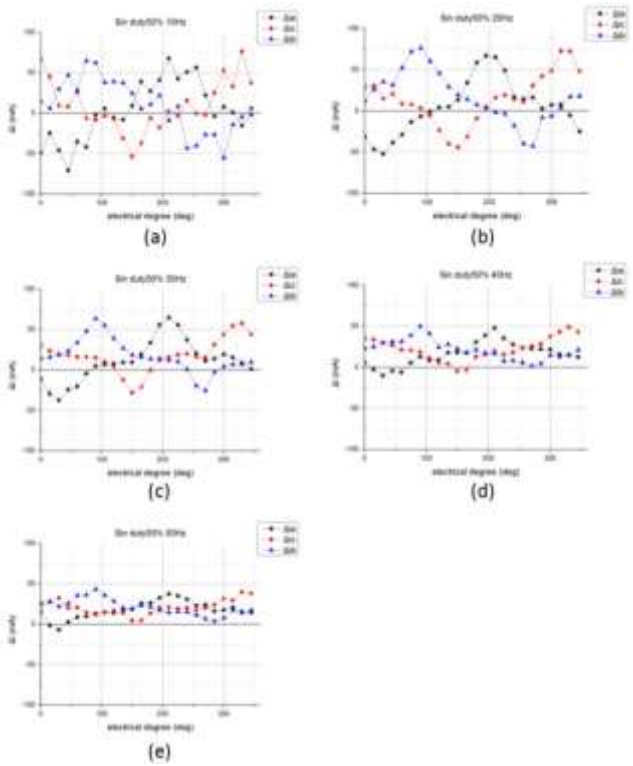


Figure 8. The relation between feedback current difference ( $\Delta i$ ) and rotation angle. The input signal is a sinusoidal function with a frequency of (a) 10 Hz, (b) 20 Hz, (c) 30 Hz, (d) 40 Hz, and (e) 50 Hz

As shown in Figure 5 rotor partition estimate accuracy increases with the three-phase current ( $\Delta i$ ) error. To improve estimate resolution, this paper uses the arctangent function to reverse the initial electrical angle. This method uses sum-to-product formula. We already know that $\Delta i_a, \Delta i_b, \Delta i_c$ each have 120 degrees difference of electrical angle. Using Eq. 21, we can obtain $\Delta i_u, \Delta i_v, \Delta i_w$ and eliminate the DC offset.

$$\begin{cases} \Delta i_u = (\Delta i_a - \Delta i_b)/\sqrt{3} \\ \Delta i_v = (\Delta i_b - \Delta i_c)/\sqrt{3} \\ \Delta i_w = (\Delta i_c - \Delta i_a)/\sqrt{3} \end{cases} \tag{21}$$

We again use the plot difference to obtain the $x, y$ for each 90 degree difference of electrical angle:

$$\begin{cases} x = \Delta i_u \\ y = (\Delta i_v - \Delta i_w)/\sqrt{3} \end{cases} \tag{22}$$

Finally, the electrical arctangent function is used to obtain the initial angle:

$$\theta_e = \arctan(\frac{x}{y}) \tag{23}$$

Figure 9 shows the relationship between the actual position and the estimated rotor position to evaluate the estimated accuracy. We use two injection frequencies of the developed method to compare with the two sine waves method. The result proves that our Sensorless Initial Rotor Position Estimation Method (Figure 9(a)) get the better result than Two Sine Waves Method [20] (Figure 9(c)) at the error of actual rotor position and the estimated value. The experimental RMS error is also calculated in Table 1, which tells the frequency of 20Hz in injection can get the most accurate rotor position.

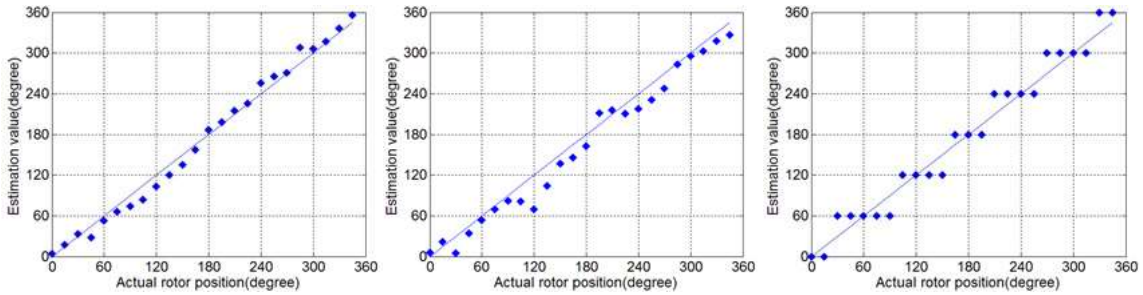


(a) (b) (c)

Figure 9. Rotor position estimates for (a) novel method with 20Hz injection frequence (b) novel method with 50Hz injection frequence (c) two sine waves method [20]

Table 1. Comparison of Different Injection Frequence and Methods

| | Novel method with 20Hz | Novel method with 50Hz | Two sine waves method |
|---|---|---|---|
| RMS Error | 11.44 | 18.95 | 18.37 |

## 6. CONCLUSION

In this paper, we analyze the methodology of Magnetic Circuit Analysis to establish an equivalent inductance model of permanent-magnet synchronous motors. With this model, different rotor positions are found to correspond to different inductor values. Therefore, The optimum injection frequency is obtained by the simulation process of the Matlab. The RMS error of the experimental shows the optimum injection frequency(20Hz), which is much lower than the other injection frequency and injection method. Our method can help the driver developer in their early motor developmrnt process to avoid using trial and error to find the optimum injection frequency. Besides, using this injection method, there is only one frequency injection applied. This can exempt the excessive starting of the motor that would usually generate the noise and vibration. We conclude that this novel invention can be widely used in the intelligent appliances, that the permanent magnet synchronous motor is one of the most important components in the device.

## REFERENCES

[1] R. Wu and G. R. Slemon, "A permanent magnet motor drive without a shaft sensor," *IEEE Trans. Industry Application*, vol/issue: 27(5), pp. 1005-1011, 1991.
[2] Z. Chen, *et al.*, "An extended electromotive force model for sensorless control of interior permanent-magnet synchronous motors," *IEEE Trans. Industrial Electronics*, vol/issue: 50(2), pp. 288-295, 2003.
[3] S. Ogasawara and H. Akagi, "An approach to position sensorless drive for brushless DC motors," *IEEE Trans. Industry Application*, vol/issue: 27(5), pp. 928-933, 1991.
[4] H. Kim, *et al.*, "A novel method for initial rotor position estimation for IPM synchronous machine drives," *IEEE Trans. Industry Application*, vol/issue: 40(5), pp. 1369-1378, 2004.
[5] Y. R. Kim, *et al.*, "Speed sensorless vector control of induction motor using extended Kalman filter," *IEEE Trans. Industry Application*, vol/issue: 30(5), pp. 1225-1233, 1994.
[6] S. Bolognani, *et al.*, "Sensorless full-digital PMSM drive with EKF estimation of speed and rotor position," *IEEE Trans. Industrial Electronics*, vol/issue: 46(1), pp. 184-191, 1999.
[7] E. Mese and D. A. Torrey, "An Approach for Sensorless Position Estimation for Switched Reluctance Motors Using Artifical Neural Networks," *IEEE Trans. Power Electronics*, vol/issue: 17(1), pp. 66-75, 2004.
[8] A. S. Tirban, *et al.*, "Motion-Sensorless Control of BLDC-PM Motor with Offline FEM-Information-Assisted Position and Speed Observer," *IEEE Trans. Industry Application*, vol/issue: 48(6), pp. 1950-1958, 2012.
[9] S. Kaliappan and R. Rajeswari, "A Novel Approach of Position Estimation and Power Factor Corrector Converter Fed BLDC Motor," *International Journal of Power Electronics and Drive System* (IJPEDS), vol/issue: 5(3), pp. 415-423, 2015.
[10] S. Alahakoon, *et al.*, "DSP-Based Sensorless Speed Control of a Permanent Magnet," *International Journal of Power Electronics and Drive System (IJPEDS)*, vol/issue: 4(3), pp. 281-289, 2015.
[11] A. Gouichiche, *et al.*, "Sensorless Sliding Mode Vector Control of Induction Motor Drives," *International Journal of Power Electronics and Drive System (IJPEDS)*, vol/issue: 2(3), pp. 217-284, 2012.
[12] H. Glaoui, *et al.*, "Speed Synchronisation of web winding System with Sliding Mode Control," *International Journal of Power Electronics and Drive System (IJPEDS)*, vol/issue: 3(2), pp. 155-169, 2012.
[13] M. E. Haque, *et al.*, "A Sensorless Initial Rotor Position Estimation Scheme for a Direct Torque Controlled Interior Permanent Magnet Synchronous Motor Drive," *IEEE Trans. Power Electronics*, vol/issue: 18(6), pp. 1376-1383, 2003.

[14] T. Noguchi, *et al.*, "Initial rotor position estimation method of sensorless PM motor with no sensitivity to armature resistance," *IEEE Trans. Industrial Electronics*, vol/issue: 45(1), pp. 118-125, 1998.
[15] R. Dhaouadi, *et al.*, "Design and implementation of an extended Kalman filter for the state estimation of a permanent magnet synchronous motor," *IEEE Trans. Power Electronics*, vol/issue: 6(3), pp. 491-497, 1991.
[16] N. Matsui, "Sensorless PM brushless DC motor drives," *IEEE Trans. Industrial Electronics*, vol/issue: 43(6), pp. 300-308, 1996.
[17] N. Matsui and T. Takeshita, "A novel starting method of sensorless salient-pole brushless motor," *IEEE Industry Applications Society Annual Meeting (IEEE-IAS Conf.). Denver. CO*, vol. 1, pp. 386-392, 1994.
[18] P. B. Schmidt, *et al.*, "*Initial rotor angle detection of a non-salient pole permanent-magnet synchronous motor drive,"* IEEE Industry Applications Society Annual Meeting (IEEE-IAS Conf.), New Orleans, vol. 1, pp. 459-463, 1997.
[19] M. Tursini, *et al.*, "Initial rotor position estimation method for PM motors," *IEEE Trans. Industry Application*, vol/issue: 39(6), pp. 1630-1640, 2003.
[20] K. Hatakeyama, *et al.*, "Accurate estimation of initial rotor position for brushless DC motor position sensorless drive," *IEEE Electrical Machines and Systems (ICEMS)*, Tokyo, vol. 1, pp. 1-6, 2009.
[21] S. J. Wang and S. K. Lin, "Analytical Prediction of the Incremental Inductance of the Permanent Magnet Synchronous Motors," *IEEE Trans. Magnetics*, vol/issue: 40(4), pp. 2044-2046, 2004.